RESEARCH ARTICLE

Biochemical and cellular studies of three human 3-phosphoglycerate dehydrogenase variants responsible for pathological reduced L-serine levels

Giulia Murtas[1] | Elena Zerbini[1] | Valentina Rabattoni[1] | Zoraide Motta[1] |
Laura Caldinelli[1] | Marco Orlando[2] | Francesco Marchesani[3] |
Barbara Campanini[4] | Silvia Sacchi[1] | Loredano Pollegioni[1] [ORCID]

[1]Department of Biotechnology and Life Sciences, University of Insubria, Varese, Italy

[2]Department of Biotechnology and Biosciences, University of Milano-Bicocca, Milan, Italy

[3]Department of Medicine and Surgery, University of Parma, Parma, Italy

[4]Department of Food and Drug, University of Parma, Parma, Italy

Correspondence
Loredano Pollegioni, Department of Biotechnology and Life Sciences, University of Insubria, via J.H. Dunant 3, 21100 Varese, Italy.
Email: loredano.pollegioni@uninsubria.it

Abstract

In the brain, the non-essential amino acid L-serine is produced through the phosphorylated pathway (PP) starting from the glycolytic intermediate 3-phosphoglycerate: among the different roles played by this amino acid, it can be converted into D-serine and glycine, the two main co-agonists of NMDA receptors. In humans, the enzymes of the PP, namely phosphoglycerate dehydrogenase (hPHGDH, which catalyzes the first and rate-limiting step of this pathway), 3-phosphoserine aminotransferase, and 3-phosphoserine phosphatase are likely organized in the cytosol as a metabolic assembly (a "serinosome"). The hPHGDH deficiency is a pathological condition biochemically characterized by reduced levels of L-serine in plasma and cerebrospinal fluid and clinically identified by severe neurological impairment. Here, three single-point variants responsible for hPHGDH deficiency and Neu-Laxova syndrome have been studied. Their biochemical characterization shows that V261M, V425M, and V490M substitutions alter either the kinetic (both maximal activity and K_m for 3-phosphoglycerate in the physiological direction) and the structural properties (secondary, tertiary, and quaternary structure, favoring aggregation) of hPHGDH. All the three variants have been successfully ectopically expressed in U251 cells, thus the pathological effect is not due to hindered expression level. At the cellular level, mistargeting and aggregation phenomena have been observed in cells transiently expressing

---

Abbreviations: 3PG, 3-phosphoglycerate; 3PHP, 3-phosphohydroxypyruvate; αKG, α-ketoglutarate; ACT, aspartate kinase-chorismate mutase-tyrA prephenate dehydrogenase; ANS, 8-anilino-1-naphthalenesulfonic acid; ASB, allosteric substrate binding; CD, circular dichroism; D-Asp, D-aspartate; D-Ser, D-serine; DMEM, Dulbecco's modified Eagles' medium; FBS, fetal bovine serum; GAPDH, glyceraldehyde-3-phosphate dehydrogenase; Gly, glycine; hPHGDH, human phosphoglycerate dehydrogenase; HPLC, high performance liquid chromatography; K_d, dissociation constant; IPTG, isopropyl β-D-1-thiogalactopyranoside; L-Asp, L-aspartate; L-Glu, L-glutamate; L-Ser, L-serine; MacTel, Macular Telangiectasia type 2; MtPHGDH, *Mycobacterium tuberculosis* PHGDH; NAC, *N*-acetyl-L-cysteine; NMDA, *N*-methyl-D-aspartate; NLS, Neu-Laxova syndrome; OPA, *o*-phtaldialdehyde; PBS, phosphate buffered saline; PHGDH, phosphoglycerate dehydrogenase; PP, phosphorylated pathway; PSAT, 3-phosphoserine aminotransferase; PSP, 3-phosphoserine phosphatase; ROI, regions of interest; SNPs, single nucleotide polymorphisms; TBS, tris-buffered saline; TCA, trichloroacetic acid.

------

the pathological protein variants, as well as a reduced L-serine cellular level. Previous studies demonstrated that the pharmacological supplementation of L-serine in hPHGDH deficiencies could ameliorate some of the related symptoms: our results now suggest the use of additional and alternative therapeutic approaches.

1 | INTRODUCTION

Phosphoglycerate dehydrogenase (PHGDH, EC 1.1.1.95) catalyzes the first step of the L-serine synthetic pathway (the so-called phosphorylated pathway, PP) by oxidizing the glycolytic intermediate 3-phosphoglycerate (3PG) to 3-phosphohydroxypyruvate (3PHP) using NAD^+/NADH as cofactor (Scheme 1). This product is subsequently converted to 3-phosphoserine by 3-phosphoserine aminotransferase (PSAT) and then to L-serine via 3-phosphoserine phosphatase (PSP).[1] The equilibrium of the reaction catalyzed by PHGDH lies far in the direction of 3PG[2,3]: *in vivo*, the reaction proceeds in the direction of serine synthesis because the product 3PHP is continuously consumed by the subsequent steps. This provides a mechanism that preserves 3PG for later steps in glycolysis by using it in the PP when L-serine is required/consumed only.

In humans, L-serine (L-Ser) is considered as a non-essential amino acid, since it can be produced from glucose and glycine; it plays a central role in the metabolism participating in the synthesis of nucleotides, lipids, various amino acids, antioxidants and cofactors, and acting as a main donor of one-carbon units.[4] In the brain, L-serine (mainly synthesized endogenously owing to the poor transport of plasma serine across the blood–brain barrier) is the precursor of D-serine and can be converted into glycine, the two main co-agonists of *N*-methyl-D-aspartate (NMDA) receptors in the hindbrain.[5,6] Moreover, due to its involvement in cell growth and in one-carbon unit metabolism, it plays a main role in promoting tumorigenesis in many cancers, see References 7–9. Therefore, the control of L-serine cellular level represents a suitable target for promising anti-cancer and drug resistance approaches.[10]

From a structural point of view, the human PHGDH (hPHGDH) belongs to the most complex type I group. In addition to the N-terminal region (residues 1–308)
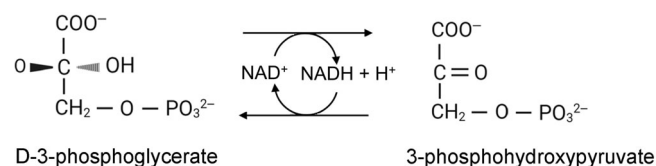
responsible for dimerization and formation of the substrate and the nucleotide-binding sites, it contains two regulatory domains (residues 309–533): the ACT (aspartate kinase-chorismate mutase-tyrA prephenate dehydrogenase) and ASB (allosteric substrate binding) domains.[1,11] Only the structure of the hPHGDH dimer consisting of the N-terminal region is known (PDB 2g76). The closest hPHGDH homolog is the one from *Mycobacterium tuberculosis* (MtPHGDH, PDB 1ygy): it is a tetramer, for which the ACT domain is known to play a feedback inhibition by L-Ser and the ASB domain mediates the tetramerization and is regulated by substrate binding.[12,13] The structure and function of these two regulatory domains in hPHGDH have remained elusive. The template-free AlphaFold structure prediction[14] of the full length hPHGDH monomer (https://alphafold.ebi.ac.uk/entry/O43175) is shown in Figure 1A.

We recently expressed in *Escherichia coli* cells the full-length recombinant hPHGDH and characterized its main biochemical properties.[3] The kinetic parameters were determined in both the forward and reverse direction: notably, neither 3PHP, L-Ser, D-serine (D-Ser), nor glycine (Gly) inhibited the reaction on 3PG. hPHGDH is a promiscuous enzyme, active on various carboxylic acids containing 3–5 carbon atoms; it is present in solution as a homotetramer and likely exists as a mixture of different conformations. Alongside, our very recent studies on astrocytes differentiated from human neural stem cells revealed that the enzymes of the PP produce a metabolic assembly (a "serinosome") that should undergo clustering in response to varying metabolic stimuli.[15]

The hPHGDH deficiency (MIM 6018153) is a pathological condition biochemically characterized by reduced levels of L-Ser in plasma and cerebrospinal fluid and clinically identified by severe neurological impairment[16]; a list of pathological single nucleotide polymorphisms (SNPs) reported in the NCBI database is given in Table 1. Twenty-one different mutations were found responsible for hPHGDH deficiency and Neu-Laxova Syndrome (NLS): 16 were caused by a missense substitution,[1] two by a nonsense substitution, and three were frameshift mutations. In a pioneering study, five patients from three families have been described, all presenting with congenital microcephaly.[16–18] These patients showed psychomotor retardation and severe intractable seizures appeared

SCHEME 1 The reversible reaction catalyzed by PHGDH.
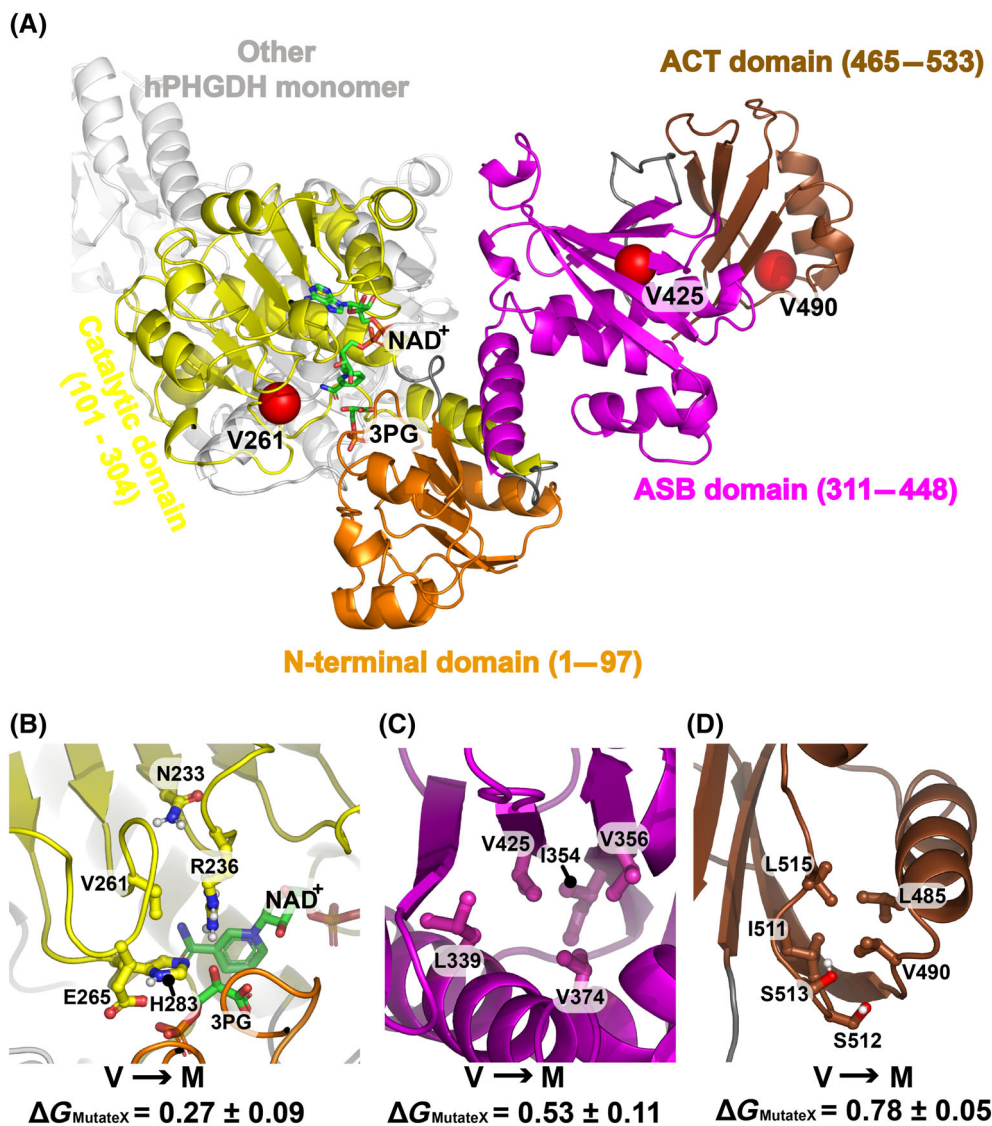
FIGURE 1 Model of the structure of dimeric hPHGDH. (A) A full-length chain monomer built by merging the experimental solved structure PDB 2g76 with the AlphaFold predicted model (https://alphafold.ebi.ac.uk/entry/O43175). The PHGDH structure PDB ID 6cwa was used as a template to add 3PG and NAD^+ (represented in sticks with carbon, oxygen and nitrogen atoms colored in green, red, and blue, respectively) using AlphaFill.[48] The positions corresponding to substitutions investigated in this work have been highlighted by red spheres. (B–D) The residues interacting for more than 50% of sampled conformers (Table S4) with the positions V261 (B), V425 (C), and V490 (D) are shown as ball-and-sticks. The predicted average $\Delta G_{MutateX} \pm$ SD (kcal/mol) value upon Val to Met substitution over sampled conformations is reported: a positive $\Delta G_{MutateX}$ value indicates a destabilization with respect to the wild-type sequence. The images were prepared with open-source PyMOL v2.5.0 (https://github.com/schrodinger/pymol-open-source).

during the first year of life; cataracts, hypogonadism, adduction of the thumbs, megaloblastic anemia, and thrombocytopenia were likely present. Notably, the pharmacological supplementation of L-Ser could ameliorate the convulsions, see Reference 19. Assays on cell lysates of cultured patient skin fibroblasts revealed reduced hPHGDH activities: <20% residual enzyme activity was consistently detected and classified as anabolic amino acidopathy.[16] Concerning NLS, a rare hereditary disorder leading to perinatal lethality, in two Chinese families with perinatal fatal disorders, gene sequencing identified recurrent missense mutations in two genes of the PP

(PHGDH and PSAT1).[20] In infants, the serum L-Ser level was 27.9 versus 60–360 μM for healthy controls; in one family the heterozygous mutation yielding the V490M variant was identified. Furthermore, Macular Telangiectasia type 2 (MacTel) is a progressive, late-onset retinal degenerative disease showing a decreased level of serine in blood and increased circulating levels of deoxysphingolipids (a toxic ceramide species): recently, rare functional variants of the hPHGDH enzyme were discovered, accounting for ~3.2% of affected individuals.[21] Among the identified variants, the V425M and the V490M substitutions have been recognized, showing at the cellular

TABLE 1 List of SNPs reported in NCBI database (in bold the three mutations investigated in this article).

Variant	rs number	Associated pathology (reference)	Localization	Functional impact prediction–PolyPhen-2[a]	gMVP rankscore[b]
E40Q	rs1650721954	L-Ser deficiency No publications	Substrate-binding site	Benign	0.69
G140R	rs587777770	NLS[42,43]	Nucleotide-binding site	Probably damaging	0.97
R163Q	rs587777483	NLS[42]	Nucleotide-binding site	Probably damaging	0.87
G237R	rs1341545186	L-Ser deficiency No publications	Nucleotide-binding site	Probably damaging	0.96
V261M (homozygous)	rs267606947	L-Ser deficiency[40]	Nucleotide-binding site	Probably damaging	0.86
E265K	rs587777774	NLS[44]	Nucleotide-binding site	Probably damaging	0.95
A286P	rs587777775	NLS[44]	Substrate-binding site	Probably damaging	0.90
Q292K	rs749134845	L-Ser deficiency No publications	Substrate-binding site	Probably damaging	0.88
E297K	rs1489498331	L-Ser deficiency No publications	Substrate-binding site	Benign	0.62
Q359E	rs1652150288	L-Ser deficiency No publications	ASB domain	Benign	0.71
G377S	rs267606948	L-Ser deficiency[40]	ASB domain	Probably damaging	0.93
V425M (homozygous)	rs121907988	L-Ser deficiency[18,38]	ASB domain	Possibly damaging	0.68
G429V	rs1652276195	NLS[45]	ASB domain	Possibly damaging	0.86
V490M (homozygous)	rs121907987	L-Ser deficiency[38]	ACT domain at dimer interface	Possibly damaging	0.79

[a]Reference [46]. The HumDiv dataset was used to evaluate rare alleles at loci involved in complex phenotypes.

[b]The rank score ranges from 0 to 1. At a minimum threshold of 0.7, gMVP showed the best positive predictive performance in detecting pathogenic single-site missense mutations among predictors.[47]

level >75% decreased activity and 50% decreased expression level.

In the present study, we performed a biochemical and cellular characterization of three recombinant full-length hPHGDH variants associated with pathological states, that is, V261M, V425M, and V490M (located in the cofactor binding, ASB and ACT domain, respectively, Figure 1A). This with the aim to clarify the consequences of the pathogenic mutations on the physiological production of L-Ser through the PP (and, in turn, of D-Ser) and to propose suitable targeted therapeutic approaches.

2 | EXPERIMENTAL PROCEDURES

2.1 | Preparation and expression of hPHGDH variants in *E. coli*

Mutagenesis reactions were performed on the pETM-His-hPHGDH expression plasmid[3] using the protocol reported in Reference 22 and the primers reported in Table S1. The highest production yields for the hPHGDH variants were obtained by growing transformed *E. coli* BL21(DE3) cells until an OD_{600nm} value of 0.6 at 37°C before adding isopropyl β-D-1-thiogalactopyranoside (IPTG), followed by incubation under the conditions reported in Table S2. Cells were harvested by centrifugation (6000 *g*, 30 min, 4°C) and stored at −20°C. The His-tagged V261M hPHGDH variant was purified by HiTrap Chelating chromatography (Amersham Biosciences, Amersham, UK) as reported for the wild-type enzyme in Reference 3. The His-tagged V425M and V490M variants (as well as the wild-type hPHGDH) were purified from inclusion bodies, using the protocol suggested by GE Healthcare (GE Healthcare, Chicago, IL; application note 18-1134-37AC).

The final enzyme preparations were stored at −80°C in 50 mM Hepes, pH 7, 5% (v/v) glycerol. The enzyme concentration was determined spectrophotometrically by using the theoretical extinction coefficient at 280 nm ($40.45 \text{ mM}^{-1} \text{ cm}^{-1}$).[3]

2.2 | Activity assay and kinetic measurements

The hPHGDH activity in the physiological direction was determined by monitoring the time course of NADH fluorescence intensity (recording the emission at 450 nm following excitation at 360 nm) at 37°C in 96-well plates with the Infinite 200 Pro reader (TECAN, Männedorf, Switzerland). The assays were performed using 0.04 μg hPHGDH (0.007 μM) in 25 mM Hepes, pH 7.0, 2.5 mM 3PG and in the presence of 1.5 mM NAD$^+$ and 200 mM hydrazine or 1.7 μM PSAT in the presence of 30 mM L-glutamate (L-Glu)—hydrazine and PSAT are required to drive the reaction forward. The latter assay was used to determine the apparent kinetic parameters on 3PG and NAD$^+$: K_m and k_{cat} values were calculated according to a classical Michaelis–Menten equation using the initial velocity values determined at increasing substrate concentrations:

$$v_0 = k_{cat} \times [E_t] \times [S]/([S] + K_m) \qquad (1)$$

or the equation modified to account for substrate inhibition:

$$v_0 = k_{cat} \times [E_t] \times [S]/([S] + K_m + [S]^2/K_i) \qquad (2)$$

The assay was also performed in "physiological conditions" in 50 mM Hepes pH 7.0, 100 mM KCl, 0.2 mM MgCl$_2$ at 37°C, using 0.82 μM hPHGDH, 1.14 μM PSAT, in the presence of 2 mM L-Glu and 0.3 mM NAD$^+$.[15]

The hPHGDH activity in the reverse direction was determined by monitoring the decrease in NADH fluorescence intensity over time at 37°C. The assays were performed using 0.6 μg of enzyme (0.82 μM) in 25 mM Hepes, pH 7.0, different amounts of 3PHP or α-ketoglutarate (αKG) and in the presence of 5 mM NADH or of 0.5 mM 3PHP and different amounts of the cofactor. Data were fitted using Equations (1) and (2) (see above).

The overall reaction from 3PG to L-Ser was recorded in 50 mM Hepes buffer, pH 7.0, and at 37°C, in the presence of 0.1 mg/mL BSA, 100 mM KCl, and 0.2 mM MgCl$_2$.[15] The reaction mixture contained 0.82 μM hPHGDH, 1.14 μM PSAT, 0.12 μM PSP, 0.3 mM NAD$^+$, 0.54 mM 3PG, and 2 mM L-Glu. The progression of the reaction was recorded by the continuous detection of NADH production following its fluorescence emission at 450 nm upon excitation at 340 nm. The simulation of the kinetic traces for the reconstituted PP in terms of NADH production was carried out by Copasi 4.37 software (http://www.copasi.org). In detail: the reaction of hPHGDH was considered a bi–bi reversible reaction, with an equilibrium constant ≤0.002; the reaction of PSAT was considered a ping–pong reaction, with an equilibrium constant of 10–40; the reaction of PSP was considered as a Henri–Michaelis Menten irreversible reaction[15]; the kinetic constants reported in Table 2 were used for the simulations.

2.3 | Determination of the oligomerization state

Size-exclusion chromatography was carried out using a Superdex 200 Increase column (Cytiva, Milano, Italy; 1–600 kDa separation range) on an AKTA system. The column was equilibrated in 25 mM Hepes, pH 7.0, 0.15 M NaCl, and loaded of 200 μL of 1 mg/mL hPHGDH. The presence of the dehydrogenase in the eluted peaks was evaluated by SDS–PAGE and Western blot analyses by using a specific anti-His antibody (diluted 1:200, Santa Cruz Biotechnology Inc., Dallas, TX). Furthermore, a Superose 6 column (Cytiva; 5–5000 kDa separation range) was also used under identical conditions.

2.4 | Spectral measurements

Circular dichroism (CD) spectra were recorded using a Jasco J-815 spectropolarimeter (Jasco Co., Cremella, Italy) in 10 mM potassium phosphate, pH 7.0, 15°C. The cell pathlength was 0.1 cm for measurements in the 200- to 250-nm region (0.1 mg protein/mL) and 1 cm for measurements in the 250- to 350-nm range (0.5 mg protein/mL).[23]

Protein fluorescence spectra were measured at 0.06–0.10 mg/mL protein concentration in 10 mM potassium phosphate, pH 7.0, 15°C; spectra were recorded using a Jasco FP-750 instrument and were corrected for the buffer contribution.

The cofactor dissociation constants (K_d values) were estimated by titrating 1 μM enzyme with increasing amounts of NAD$^+$ or NADH and following the protein fluorescence quenching at 330 nm. K_d values were determined by fitting the data to a hyperbolic function.[24] The same method was used to determine K_d values for the hydrophobic fluorescent probe 8-anilino-1-naphthalenesulfonic acid (ANS), used to investigate the exposure of hydrophobic regions.[25]

Temperature-ramp experiments were performed in 10 mM potassium phosphate, pH 7.0, with a temperature gradient (0.5°C/min).[26] For this a software-driven, Peltier-equipped fluorimeter recorded the protein fluorescence change at 330 nm and a CD spectropolarimeter followed the signal at 220 nm.

2.5 | Limited proteolysis

The hPHGDH at 0.4 mg/mL was incubated at 25°C in 50 mM Hepes, pH 7, 5% (v/v) glycerol in the presence of 5% (w/w) trypsin (Roche, Basel, Switzerland) with or without 500 mM sodium tartrate. At different times (0, 5, 10, 20, 30, 60, and 120 min), 8 μg of protein was diluted in the SDS-PAGE sample buffer, heated at 95°C for 5 min and analyzed by SDS-PAGE.

2.6 | Constructs for hPHGDH variants over-expression in U251 mammalian cells

Missense mutations V261M, V425M, and V490M were introduced in pcDNA3.1+/C-(K)-DYK-hPHGDH-1xFLAG (U362CGJ270-1, GenScript Piscataway, NJ) using the Quickchange Lightning™ site-directed muta-genesis kit (Agilent Technologies, Santa Clara, CA) and the primers listed in Table S1. All constructs were verified by sequencing.

The U251 human glioblastoma cell line (ATCC) was chosen for this study since it endogenously expresses the PP's enzymes. Cells were cultured in Dulbecco's Modified Eagles' Medium (DMEM, Euroclone, Pero, Milan, Italy) supplemented with 10% fetal bovine serum (FBS), 1 mM sodium pyruvate, 2 mM L-glutamine, 1% non-essential amino acid, 1% penicillin–streptomycin, and 1% amphotericin B, at 37°C in 5% CO_2. Cells were daily evaluated at the microscope for vitality and density: medium was changed two to three times per week. Subculturing was performed when cells reached 80%–90% of confluence, by treatment with EDTA trypsin.

2.7 | Transient transfection

For Western blot and High-Performance Liquid Chromatography (HPLC) analyses, U251 cells were seeded into 6-well plates (2×10^5 cells/well); for immunolocalization studies the same cells were seeded into 24-well plates (0.5×10^5 cells/well) on gelatinized coverslips (diameter 12 mm; Thermo Scientific, Waltham, MA). At 24 h after seeding, cells were transfected with 2 and 0.5 μg plasmid DNA (pcDNA3.1-hPHGDH-1xFLAG wild-type, V261M, V425M e V490M) for cells in 6- and 24-well plates, respectively, using a 3:1 ratio of Lipofectamine 2000 (Invitrogen) to DNA. The cells were either collected or fixed (on coverslips) at different times after transfection (24, 48, and 72 h). Fixation was performed after extensively washing with phosphate buffered saline (PBS, 10 mM dibasic sodium phosphate, 2 mM monobasic potassium phosphate, 137 mM NaCl, 2.7 mM KCl,

pH 7.4) by incubating coverslips in 4% *p*-formaldehyde for 10 min at room temperature.

Immunostaining and confocal analysis allowed to evaluate the transfection efficiency: for wild-type protein and pathological variants, the fraction of transfected cells (stained for the anti-FLAG antibody) over the total number of cells (determined by counting nuclei stained by the DRAQ5 dye) ranged between 21 and 27% at 24 and 48 h after transfection, and slightly decreased at 72 h (14–16%), with the only exception of cells expressing the V425M hPHGDH for which the value remained unchanged.

For HPLC analyses, cell pellets were resuspended in 0.2 M trichloroacetic acid (TCA), incubated in an ultrasound bath for 20 min and centrifuged at 16,000 g at 4°C for 20 min. Supernatants were used for HPLC analyses, while pellets, representing the protein fraction, were resuspended in 1% SDS, incubated 10 min at room temperature, in an ultrasound bath for 20 min, and centrifuged at 16,000 g at 4°C for 10 min. The supernatants containing soluble proteins were quantified using Bradford protein assay (Bio-Rad, Hercules, CA); aliquots of supernatant samples corresponding to 20 μg of total proteins were analyzed by Western blot.

For Western blot analyses, protein samples diluted in SDS-PAGE sample buffer and boiled for 5 min were loaded onto a 12% SDS-PAGE gel along with molecular weight markers (Page Ruler Prestained Protein Ladder, Thermo Scientific, Waltham, MA) and mixtures containing different amounts (ng) of recombinant proteins, as quantitative reference standards. After electrophoresis, proteins were transferred onto a PVDF membrane (Millipore, Burlington, MA) via electroblotting. The membrane was incubated with Tris-buffered saline blocking solution (TBS, 0.1% Tween-20, 4% non-fat dry milk) overnight at 4°C and, to allow the detection of different proteins in the same samples, cut into three pieces: (1) 150–100 kDa range, containing hPHGDH and recombinant hPHGDH (wild-type and V261M, V425M, V490M variants)-FLAG, 56.7 and 57.6 kDa, respectively; (2) 36–50 kDa range, containing PSAT and glyceraldehyde-3-phosphate dehydrogenase (GAPDH, used as loading control), 40.5 and 37 kDa, respectively; and (3) 23–36 kDa range, containing PSP (25 kDa). The membrane was then incubated with primary antibodies appropriately diluted in TBS, 0.05% Tween-20, 2% non-fat dry milk and, after extensive washes, with secondary antibodies diluted in TBS, 0.05% Tween-20 (Table S3). Fluorescent signals corresponding to the proteins of interest were detected and analyzed by an Odyssey Fc Imaging System instrument (LI-COR Biosciences, Lincoln, NE).

The expression levels of the PP's enzymes in U251 transfected cells compared with non-transfected cells

(control) were quantified by measuring relative densities of protein bands using Image Studio Lite software (LI-COR Biosciences). In these analyses, the density values obtained for each of the three bands corresponding to PHGDH, PSAT, and PSP were normalized to the density of the band recognized by the anti-GAPDH antibody.

2.8 | HPLC analyses

To evaluate the content of L-Ser, Gly, D-Ser, L-aspartate (L-Asp), and D-aspartate (D-Asp) in U251 cells transfected with the constructs for the ectopic expression of hPHGDH wild-type, V261M, V425M and V490M compared with controls (non-transfected cells), 10 μL of the TCA-treated supernatants were neutralized with 0.2 M NaOH and subjected to precolumn derivatization with 20 μL of 74.5 mM o-phthaldialdehyde (OPA) and 30.5 mM N-acetyl L-cysteine (NAC) in 50% methanol. The separation was carried out by reversed-phase HPLC on a Symmetry C8 column (4.6 × 250 mm, Waters S.p.A) under isocratic conditions (0.1 M sodium acetate buffer, pH 6.2, 1% tetrahydrofuran, 1 mL/min flow rate). A washing step at 50% of 0.1 M sodium acetate buffer, 47% acetonitrile, and 3% tetrahydrofuran was performed after each run. Metabolite identification was based on the comparison of the retention times of the peaks present in the sample chromatograms with the retention times of the peaks corresponding to L-Ser, Gly, D-Ser, L-Asp, and D-Asp, which were preliminarily and separately analyzed as external standards. Peak identity was confirmed by the selective degradation of the D-enantiomers by M213R RgDAAO variant.[27] Quantification of amino acids was based on calibration curves obtained analyzing known quantities of the external standards. The total amount of amino acids detected in cell extracts was normalized by the total protein content, the number of cells and considering the expression levels of each of the three PP's proteins.

2.9 | Confocal analyses

To analyze the subcellular localization of the hPHGDH proteins, p-formaldehyde-fixed U251-hPHGDH wild-type-, V261M-, V425M-, V490M-1xFLAG, and U251 non-transfected cells were permeabilized and the unspecific binding sites were blocked by incubation in PBS supplemented with 0.2% Triton X-100 and 4% horse serum. hPHGDH-1xFLAG proteins were subsequently stained using rabbit polyclonal anti-FLAG antibody (Table S3). Cells were incubated with primary antibodies overnight at 4°C and, after extensive washing in PBS supplemented with 1% horse serum, with anti-rabbit Alexa 546 antibody (1:1000, ThermoScientific, Waltham, MA) diluted in PBS,

0.1% Triton X-100. After further washing in PBS, cells were also stained with Phalloidin CruzFluor™ 488 Conjugate (sc-363791, Santa Cruz, Dallas, TX) and Draq5™ fluorescent probe (62251, ThermoScientific) for staining of the cytoskeleton and nucleus, respectively.

To evaluate the distributions of hPHGDH variants relatively to the endogenous PP's enzymes, double immunostainings were performed using primary antibodies mixtures containing the polyclonal rabbit anti-FLAG antibody along with either the polyclonal mouse anti-PHGDH, or mouse anti-PSAT or rabbit anti-PSP antibodies (Table S3). Double staining of hPHGDH variants and PSP was obtained by sequentially labeling the proteins with the rabbit anti-FLAG and the anti-rabbit Alexa 546 antibodies and then with the rabbit anti-PSP and the anti-rabbit Alexa 488 antibodies. Nuclei were stained with Draq5™ as above. Negative controls were performed by omitting primary antibodies, and using U251 untransfected control cells.

Immunostained coverslips were imaged using an inverted laser scanning confocal microscope (TCS SP5, Leica Microsystems, Wetzlar, Germany), equipped with a 63.0 × 1.25 NA plan apochromatic oil immersion objective. Confocal image stacks (10 sections with optimized thickness) were acquired using the LEICA TCS software with a sequential mode to avoid interference between each channel due to spectral overlap and without saturating any pixel.

The overlapping and correlation of immunofluorescence signals corresponding to the ectopically expressed hPHGDH variants and the PP's enzymes were analyzed by the JACoP plugin of Fiji (ImageJ) online open source software. Defined regions of interest (ROI) within images were processed subtracting the background and colocalization parameters were calculated. Three parameters were evaluated in the colocalization analysis: Manders' coefficients M1 and M2, well-established co-occurrence measures which simply calculate the percentage of total signal from one channel which overlaps with signal from the other (i.e., green over red channel and vice versa, respectively) and account for the fraction of the total fluorescence that co-occurs; the Pearsons' coefficient (r, computed selecting a Costes' threshold), a measure of the strength of the linear relationship between the two channels; and the correlation coefficient. Manders' coefficients were determined by adjusting the threshold of the green and red channel based on signals detected in the ROIs.

2.10 | Predicting the molecular effects of missense mutations

The AlphaFold-DB model of hPHGDH was used to provide a preliminary interpretation for the observed effects

of pathogenic single-site missense variants (V261M, V425M, V490M), especially for those at the C-terminal, since only experimental dimeric models of the N-terminal partial sequence are available to date. The experimentally solved N-terminal region from the dimeric model of truncated hPHGDH (PDB 2g76, residues 6–304) was joined to the C-terminal region extracted from the AlphaFold database (https://alphafold.ebi.ac.uk/entry/O43175, residues 311–533) by the loop refinement protocol of Modeler 10.2,[28] applied from Val304 to Ser311. Ten alternative conformations were generated using a high optimization level; the loop conformation with the best DOPE model score[29] was selected. The final model was refined by a conformational analysis: the clustENMD method[30] of ProDy package[31] was used. The model was prepared by adding hydrogen atoms at pH 7 with PDBFixer script (https://github.com/openmm/pdbfixer). The clustENMD sampling was performed with anisotropic network model normal mode and the following parameters: five generations, using the first three global modes and generating 50 conformers with an average C_α root-mean-square deviation distance of 1 Å from the parent conformer of the previous generation, and increasing by 20 the maximum number of clusters sampled at each generation (from 20 to 120). A short classical molecular dynamics simulation (8000 steps) was performed after energy minimization of each sampled conformer solvated in TIP3P water molecules and 150 mM Na^+ and Cl^- ions up to 1 nm distance by using OpenMM 7.5.1[32] under the amber ff14SB force field,[33] with a time step of 2.0 fs and at 30°C. The clustENMD analysis was performed in triplicate. To predict the role of selected positions in the wild-type enzyme, the obtained conformers were used to map the intra-protein non-covalent interactions at ≤4.0 Å distance to positions corresponding to the missense variants considered in this study. Moreover, they were used to estimate the stability effects upon substitution through the MutateX package[34] and FoldX 5.[35] The results were averaged over clustENMD sampled conformers to obtain a conformational-averaged ΔGFoldX score, called $\Delta G_{MutateX}$ in this study.

3 | RESULTS

3.1 | Prediction of alteration due to hPHGDH substitutions

The molecular effect of V261M, V425M, and V490M substitutions has been predicted by a conformational sampling of a dimeric model of the full-length hPHGDH obtained by AlphaFold and homology modeling (Figure 1A). Results suggest that the C-terminal region possesses a high degree of flexibility (Figure S1) and that all the amino acid substitutions in the pathological variants affect the protein stability: the positive $\Delta G_{MutateX}$ value is indicative of a destabilization compared with the wild-type hPHGDH (Figure 1B–D). Table S4 lists the pairwise interactions between V261, V425, and V490 during conformational sampling. Notably, V261M substitution is likely to directly affect the orientation of the catalytic residues, as well as the ability to bind the substrate and the cofactor since this residue interacts with active site residues His283 and Arg236. On the other hand, V425M and V490M substitutions are predicted to disrupt core hydrophobic interactions that are important to stabilize the fold of the ASB and ACT domains, respectively. These domains seem essential to regulate the tetrameric assembly of the wild-type enzyme.[36]

3.2 | Expression of recombinant hPHGDH variants

At first, hPHGDH variants were expressed in *E. coli* cells as N-terminal His-tagged proteins employing the same conditions used for the wild-type enzyme,[3] but the yield in terms of expressed soluble protein was too low for allowing their complete biochemical characterization. To improve the expression level of hPHGDH variants in a soluble form, the following parameters were investigated by employing a simplified factorial design approach[37]: the *E. coli* strain (i.e., BL21(DE3), BL21(DE3)Star, BL21(DE3)pLysS, or pLysE), the growth medium (LB or TB), the OD_{600nm} value at the moment of IPTG addition (0.6, 2.5, or 6), the concentration of the inducer IPTG (0.01, 0.1, 1 mM), the time of cell harvesting (0, 1, 2, 5, or 16 h), the temperature of growth after the induction of protein expression (17, 20, 25, or 37°C), and the inhibition of protein synthesis by adding kanamycin to the culture medium after removing IPTG. Best conditions in terms of protein expression for each hPHGDH variant are reported in Table S2.

The recombinant V261M hPHGDH variant has been purified from the crude extract by chromatography on a HiTrap Chelating column using the procedure previously set up for the wild-type enzyme[3]: SDS-PAGE analysis showed a single band at the expected size (~60 kDa, Figure S2) with a 95% of purity and an overall yield of 26.5 mg of pure protein/L of fermentation broth. On the other hand, the V425M and V490M hPHGDH variants were expressed as insoluble proteins in all the conditions tested. These recombinant proteins were thus purified using the protocol set up by GE-Healthcare for purification and refolding of a recombinant protein harboring an His-tag at its N-terminus from inclusion bodies, yielding

a protein preparation with a 95% of purity (Figure S2) and an overall yield of 14 and 8 mg of pure protein/L of fermentation broth for V425M and V490M, respectively.

As indicated by the activity assay on the purified recombinant variants at high (2.5 mM) 3PG concentration, these substitutions affect hPHGDH enzymatic activity: compared with the wild-type enzyme (3 and 1 U/mg protein for the enzyme isolated from the soluble fraction and the inclusion bodies, respectively) the strongest decrease in the specific activity was determined for the V425M variant (Table S2).

3.3 | Kinetic properties and substrate specificity

The reaction of recombinant hPHGDH on 3PG (forward direction) was assayed following the fluorescence signal related to the redox state of the nicotinamide cofactor and removing the 3PHP product using PSAT or 200 mM hydrazine (the latter assay was used to avoid any putative alteration related to PSAT recognition).[3] At first, a low hPHGDH concentration (0.007 μM) and saturating NAD^+ and L-Glu concentrations were used (1.5 and 20 mM, respectively). The apparent kinetic parameters were calculated according to a Michaelis–Menten equation using the initial velocity values determined at increasing substrate or cofactor concentrations. Under these conditions and using the hydrazine method, all the three hPHGDH variants showed a reduced affinity for both the substrate and the cofactor (K_m values up to 40-fold higher) and decreased k_{cat} values, resulting in a significant reduction in the kinetic efficiency compared with the wild-type enzyme. The lowest k_{cat}/K_m ratio was determined for the V425M and V490M variants (Figure S3 and Table 2), which also showed a 3PG inhibition effect. When the PSAT-PHGDH coupled assay was used, all the variants showed a decreased kinetic efficiency on 3PG and NAD^+, that for the V261M and V425M variants was mainly due to a decrease in k_{cat} value on 3PG. The kinetic parameters resembled the ones determined with the hydrazine method (Table 2). Notably, under conditions related to physiological ones (e.g., in the presence of chloride salts, and concentrations of NAD^+, L-Glu, PHGDH, and PSAT resembling the ones determined in human NSC-derived differentiated astrocytes, that is, 0.3 mM, 2 mM, 0.82 μM, and 1.14 μM, respectively),[15] significantly lower k_{cat} values were observed, while the K_m for 3PG was unchanged (see conditions 3 in Table 2). In all cases, no substrate inhibition effect was apparent.

Remarkably, when the hPHGDH reaction was assayed in the opposite direction, the effect of the different pathological substitutions was less evident (≤2.5-fold change in the related kinetic parameters compared with the wild-type enzyme) both using PHP or αKG as substrate (Figure S3 and Table 2).

The overall reaction of the three enzymes of the PP was evaluated for the wild-type and the variants of hPHGDH as NADH production.[15] By using the kinetic parameters determined at physiological conditions of the three enzymes (Table 2), a reasonable simulation of the experimental traces was generated (Figure 2). This result suggests a strong effect of the substitutions in hPHGDH on the kinetics of L-Ser production and the relevant rate-limiting role of the dehydrogenase. Furthermore, analysis of the experimental trace for V490M hPHGDH in the starting 500 s highlights a lag phase (Figure 2, inset), which is not apparent for the wild-type counterpart, pointing to complications in generating a functional complex with PSAT and PSP.

The investigation of the kinetic properties highlights a strong effect of the studied substitutions on the forward reaction catalyzed by hPHGDH, especially for the ones purified from inclusion bodies (see above).

3.4 | Cofactor binding

The dissociation constant for the nicotinamide cofactor was determined by titrating the hPHGDH variants with increasing amounts of NAD^+ or NADH and monitoring holoenzyme reconstitution following the fluorescence intensity at 330 nm. As for the wild-type enzyme, the binding of NAD^+ to hPHGDH variants was a monophasic process with similar K_d values (∼100 μM) (Table 3). Differently from the wild-type enzyme, in which the quenching in protein fluorescence intensity vs. NADH concentration follows a biphasic process,[3] the binding of NADH to hPHGDH variants was monophasic, with K_d values (80–120 μM) close to the one for the second phase of the wild-type enzyme (Table 3), and thus pointing to the absence of the inferred hPHGDH apoprotein form with an high affinity for NADH as for the wild-type enzyme.

Comparing binding and kinetic parameters for NAD^+/NADH, we conclude that the substitutions affect microscopic steps in hPHGDH catalysis and not alter the overall apoprotein–cofactor interaction.

3.5 | Protein conformation

The far-UV CD spectra of hPHGDH variants were significantly altered as compared with those of the wild-type enzyme, both in the apoprotein and in the holoenzyme forms (for both the NAD^+ and NADH complexes,

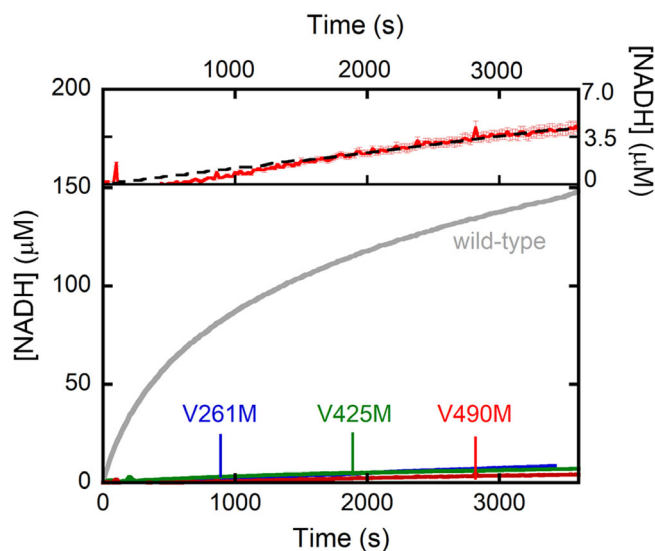**TABLE 2**   Comparison of apparent kinetic parameters of wild-type and variants of hPHGDH at 37°C and pH 7.0.

Substrate	Wild-type[a] k_{cat} (s^{-1})	K_m (mM)	k_{cat}/K_m (mM^{-1} s^{-1})	V261M k_{cat} (s^{-1})	K_m (mM)	k_{cat}/K_m (mM^{-1} s^{-1})	V425M k_{cat} (s^{-1})	K_m (mM)	k_{cat}/K_m (mM^{-1} s^{-1})	V490M k_{cat} (s^{-1})	K_m (mM)	k_{cat}/K_m (mM^{-1} s^{-1})	Assay
Forward reaction													
3PG	3.0 ± 0.1	0.36 ± 0.06	8.3	0.75 ± 0.09	0.64 ± 0.02	1.18	0.24 ± 0.04	0.69 ± 0.02 [K_i = 3.5]	0.35	0.70 ± 0.06	2.76 ± 0.03 [K_i = 4.0]	0.26	1
	5.8 ± 0.2	0.22 ± 0.06	26.1	0.39 ± 0.01	0.71 ± 0.08 [K_i = 106.2]	0.54	0.22 ± 0.03	1.3 ± 0.1 [K_i = 57.1]	0.17	0.12 ± 0.03	1.1 ± 0.1 [K_i = 12.7]	0.11	2
	0.13 ± 0.01	0.37 ± 0.07	0.351	0.0036 ± 0.0002	0.63 ± 0.18	0.0057	0.0070 ± 0.0004	0.69 ± 0.19	0.0101	0.0050 ± 0.0004	2.4 ± 0.6	0.0020	3
NAD$^+$	2.2 ± 0.3	0.10 ± 0.02	15.1	0.37 ± 0.03	0.45 ± 0.03	0.83	0.69 ± 0.05	1.0 ± 0.3	0.69	0.62 ± 0.07	4.4 ± 1.1	0.15	1
	3.0 ± 0.1	0.16 ± 0.02	19.0	0.57 ± 0.05	0.89 ± 0.02	0.64	0.43 ± 0.01	0.46 ± 0.01	0.93	0.34 ± 0.03	1.4 ± 0.3	0.24	2
Reverse reaction													
PHP	2.3 ± 0.1	0.010 ± 0.003 [K_i = 1.3]	228	0.69 ± 0.04	0.021 ± 0.005 [K_i = 8.3]	32.9	0.78 ± 0.08	0.008 ± 0.003 [K_i = 1.3]	97.5	1.19 ± 0.07	0.022 ± 0.001 [K_i = 0.34]	54.1	
αKG	1.0 ± 0.1	0.024 ± 0.007 [K_i = 13.3]	39.1	0.68 ± 0.05	0.018 ± 0.002 [K_i = 7.9]	37.8	0.47 ± 0.03	0.013 ± 0.003 [K_i = 6.9]	36.2	0.49 ± 0.04	0.019 ± 0.007 [K_i = 14.5]	25.8	
NADH	3.4 ± 0.1	0.56 ± 0.08	6.0	3.1 ± 0.4	0.99 ± 0.02 [K_i = 6.1]	3.2	1.5 ± 0.4	1.8 ± 0.1	0.81	1.5 ± 0.1	0.99 ± 0.02	1.6	

Note: Assay conditions: 50 mM Hepes pH 7.0, 1.5 mM NAD$^+$, 30 mM L-Glu, 0.007 μM PHGDH, 1.7 μM PSAT for: (1) hydrazine-based assay; (2) PHGDH-PSAT coupled assay; 50 mM Hepes pH 7.0, 100 mM KCl, 0.2 mM MgCl$_2$, 0.1 mg/mL BSA, 0.3 mM NAD$^+$, 2 mM L-Glu, 0.82 μM PHGDH, 1.14 μM PSAT for: (3) PHGDH-PSAT coupled assay under conditions resembling the physiological ones.[15]
[a] Reference 3.

Figure 3, left panels). Estimation of the secondary structure content by means of DichroWeb software (Selcon3 method) indicated that all the variants are partially unfolded. Compared with the wild-type enzyme, also the near-UV CD spectra of hPHGDH variants were altered in the apoprotein and holoenzyme form, pointing to a modification in tertiary structure (Figure 3, right panels): an increase in the signal is observed for the apoprotein of V261M variant in the 260- to 280-nm region, while a decrease is evident for the apoprotein of V425M and V490M variants. Moreover, a signal increase in the same region is evident for all the variants in the presence of NADH (Figure 3C).

The hydrophobic fluorescent probe ANS was used to investigate alterations in the exposure of hydrophobic regions.[25] Binding of this probe to hPHGDH results in a marked increase in ANS fluorescence and in a blue shift

in its emission fluorescence maximum (at 495 nm for the wild-type, V261M and V425M hPHGDHs, and at 506 nm for the V490M variant). The plot reporting the emission change versus ANS concentration (Figure S4) shows a significantly lower fluorescence intensity at saturation for the V490M variant, pointing to a comparatively lower exposure of hydrophobic regions than the wild-type enzyme. A K_d value of ~130 μM was determined for the hPHGDH wild-type and lower figures were calculated for all the pathological variants (especially for the V261M protein, Table 3), indicating an easier access of the probe to the protein hydrophobic regions.

The effect of temperature on protein folding/unfolding equilibrium was evaluated both by monitoring spectral signals related to the protein tertiary structure, that is, following the changes in protein fluorescence intensity at 330 nm (due to both Trp and Tyr residues), and by monitoring spectral signals related to the protein secondary structure, following the CD signal at 220 nm.[26] Compared with the wild-type enzyme, the signals for all the variants were significantly different: in both the analyses, and differently from the wild-type protein, the hPHGDH variants did not show a clear signal transition at increasing temperature corresponding to the denaturation step (Figure S5). This result suggests that the three hPHGDH variants are present in solution in a partially unfolded conformation.

The conformation of the variants was also evaluated by limited proteolysis. Following the addition of 5% (w/w) trypsin, the full-length 56 kDa form of hPHGDH was converted into a ~40 kDa band (in 120 min), with the transient presence of a ~47 kDa species and additional products at 28, 25, 15, and 10 kDa. Notably, the variants were already fully digested after 5 min: the 56 kDa band was no longer apparent and bands at lower masses, mostly below 25 kDa, were present (Figure S6A). In the presence of the inhibitor tartrate (500 mM), the wild-type hPHGDH was significantly protected from trypsinolysis (~60% of the full-length protein was still present after 120 min). On the other hand, the active site ligand only marginally affected the time-course proteolysis of

FIGURE 2 Comparison of experimental traces of hPHGDH wild-type (gray), V261M (blue), V425M (green), and V490M (red) variants. Inset: comparison of experimental trace (red) and simulation trace (black) of V490M hPHGDH. Conditions: 0.82 μM PHGDH, 1.14 μM PSAT, 0.12 μM PSP, 0.54 mM 3PG, 2 mM L-Glu, and 0.3 mM NAD$^+$ (37°C and pH 7.0).

TABLE 3 Comparison of cofactor and ANS binding properties of wild-type and variants of hPHGDH.

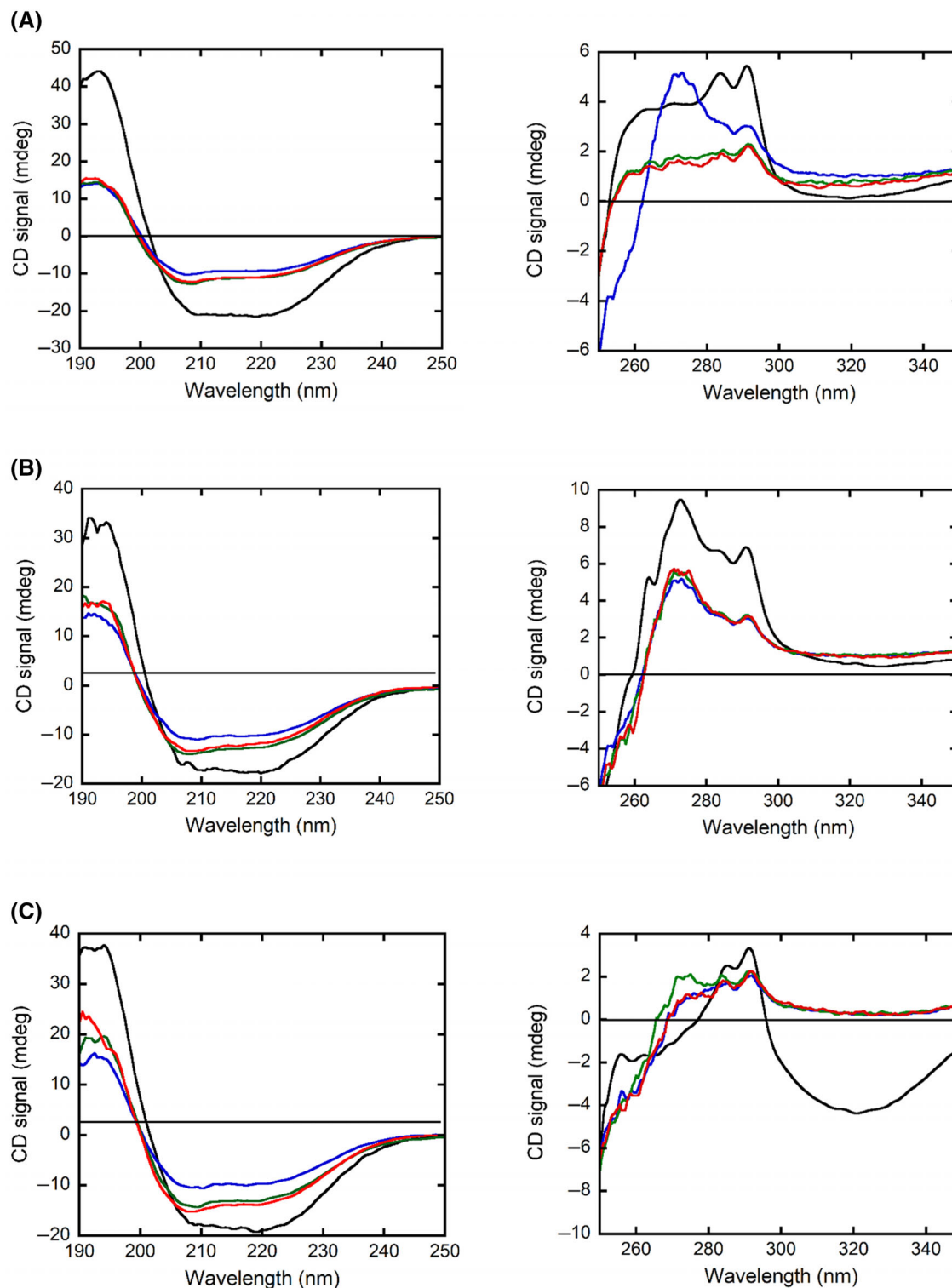|	K_d NAD$^+$ (μM)	K_d NADH (μM)	K_d ANS (μM)
Wild-type[a]	130 ± 8	0.49 ± 0.03 (first phase, 35%) 169 ± 27 (second phase, 65%)	128 ± 15
V261M	138 ± 37	120 ± 33 (monophasic)	56 ± 8
V425M	104 ± 4	91 ± 15 (monophasic)	80 ± 1
V490M	135 ± 44	82 ± 18 (monophasic)	103 ± 5

Note: K_d values were determined by monitoring the quenching of protein fluorescence at 15°C. For ANS binding see Figure S4.
[a]Reference 3.

FIGURE 3 Comparison of far-UV (left panels, 0.1 mg/mL protein) and near-UV (right panels, 0.5 mg/mL protein) CD spectra of hPHGDH wild-type and variants in the apoprotein (A) and holoenzyme form in complex with NAD^+ (B) or NADH (C). Wild-type (black); V261M (blue); V425M (green); V490M (red).

hPHGDH variants (Figure S6B). Altogether these findings indicated that the substitution of the Val residue at positions 261, 425, or 490 significantly destabilizes the protein conformation, making hPHGDH variants more accessible to trypsin.

On size-exclusion chromatography using a Superdex 200 Increase column, the recombinant wild-type hPHGDH at 1 mg/mL concentration eluted as a major peak corresponding to ~240 kDa, indicating that it behaves as a homotetramer.[3] On the contrary, all the

(A)
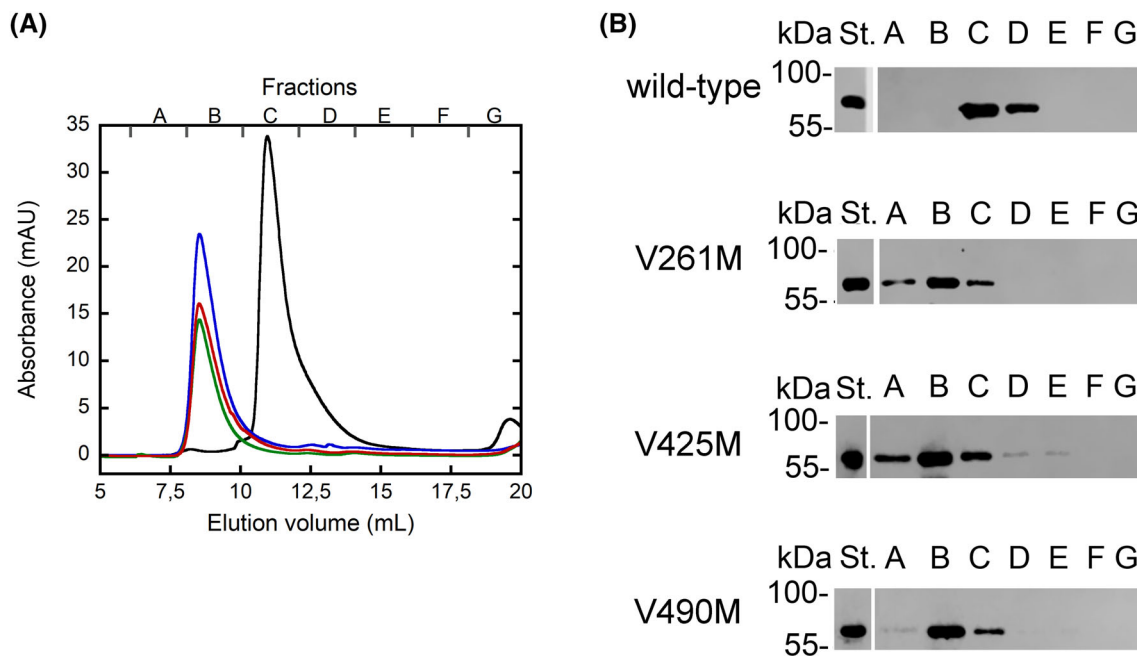
FIGURE 4 Size-exclusion chromatography analysis of hPHGDH variants. (A) Comparison of elution profiles of 1 mg/mL hPHGDH wild-type (black), V261M (blue), V425M (green) and V490M (red) in 25 mM Hepes, pH 7.0, 150 mM NaCl. (B) Western blot analysis of fractions eluted at different volumes (A to G in panel A) and of recombinant wild-type hPHGDH (0.1 μg) as standard (St.).

three variants eluted in the void volume, corresponding to a mass ≥600 kDa (Figure 4). When using a Superose 6 column, the wild-type hPHGDH still eluted as a homotetramer (~230 kDa) while all the variants eluted both in the void volume (>5000 kDa) and in a peak corresponding to ~1200 kDa, pointing to the generation of aggregates at high molecular mass. To avoid aggregation concerns, the analyses for the hPHGDH variants were performed at a protein concentration lower than 1 mg/mL.

In conclusion, the pathological substitutions alter the quaternary, tertiary and secondary structure of hPHGDH and affect its stability in solution.

3.6 | Cellular studies

To investigate the different hPHGDH variants in a context close to the physiological one (i.e., with proper folding and post-translational modifications), they were ectopically expressed in the U251 human glioblastoma cell line. These cells endogenously express the enzymes of the PP, thus allowing to study both the cellular localization of the over-expressed wild-type hPHGDH and the V261M, V425M, and V490M variants and the consequent alterations in L-Ser biosynthetic pathway. In U251 cell lysates, the endogenous amounts of PHGDH, PSAT, and PSP were 0.8 ± 0.1, 0.16 ± 0.02, and 0.19 ± 0.07 ng/μg of total proteins, respectively.

U251 cells were transiently transfected with the pcDNA3.1+/C-(K)-DYK-hPHGDH-1xFLAG encoding the wild-type enzyme or the pathological hPHGDH variants fused to a C-terminal FLAG epitope. The cellular levels of the over-expressed proteins were monitored by Western blot analysis at different times after transfection (24, 48, and 72 h) using an anti-FLAG antibody. For all hPHGDH variants maximum expression was detected at 48 h after transfection (Figure S7), with highest levels for the V425M and V490M variants. In line with these findings, an increase in total hPHGDH cellular levels compared with control untransfected U251 cells (detected by the anti-hPHGDH antibody, Figures 5A and S8) was observed: up to 3-fold for wild-type hPHGDH and up to 5.5-fold for the pathological V261M, V425M and V490M variants, at 48 h after transfection. This indicated that the pathological hPHGDH variants accumulated to a significant extent and at a higher level than the wild-type counterpart. Further Western blot analyses showed that the over-expression of hPHGDH variants, and the induced increase in total hPHGDH, also affected endogenous PSAT and PSP cellular levels (Figures 5B,C and S8). Compared with control U251 cells, increased PSAT levels (~1.5-fold) were detected at 24 h after transfection in cells expressing the different hPHGDH variants: at 48 and 72 h after transfection endogenous PSAT progressively decreased and, in U251 cells expressing V425M or V490M hPHGDH, its levels were completely restored (i. e., resembled those detected in untransfected control

(A)

(B)

(C)
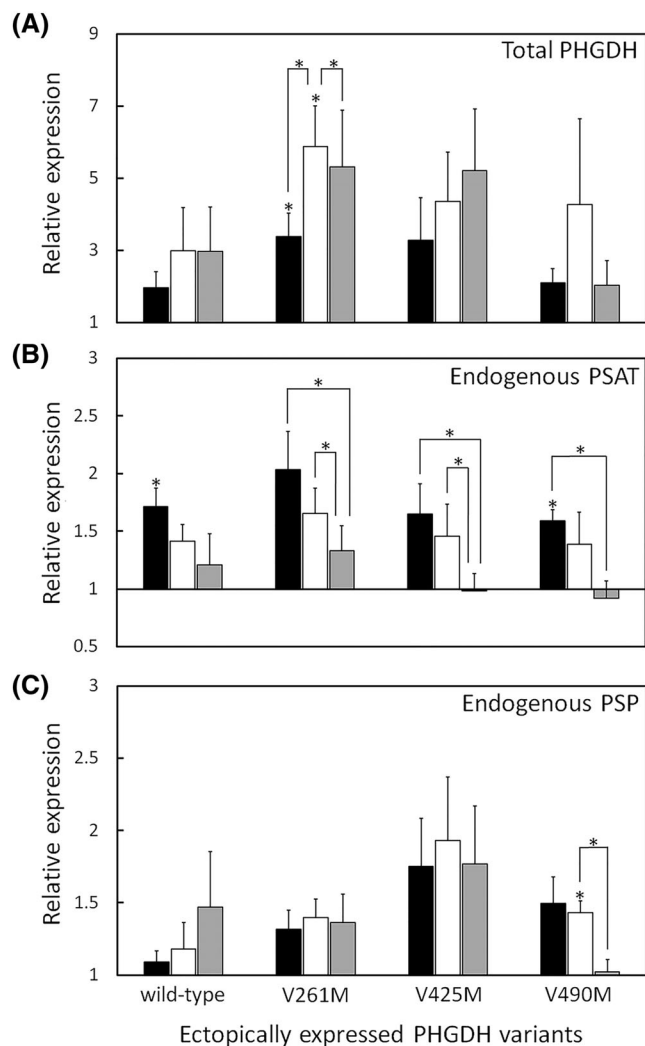
FIGURE 5 Cellular levels of the PP enzymes in U251 cells ectopically over-expressing the different PHGDH variants, as detected by Western blot analysis. Total hPHGDH (A, endogenous + ectopically expressed), and endogenous PSAT (B) and PSP (C) content is reported as relative expression (i.e., fold changes with respect to the levels of the protein detected in control, untransfected U251 cells: 0.8 ± 0.1, 0.16 ± 0.02, and 0.19 ± 0.07 ng/μg of total proteins for PHGDH, PSAT, and PSP, respectively). Total hPHGDH cellular level was evaluated using the anti-PHGDH antibody. U251 cells were analyzed at different times after transfection: 24 h (black column), 48 h (white columns), and 72 h (gray columns). The reported values represent mean ± standard errors ($n = 3$).

U251 cells). On the other hand, the expression of hPHGDH variants differently impacted on endogenous PSP cellular content. The over-expression of the wild-type hPHGDH lead to a moderate increase in PSP levels (up to 1.5-fold compared with control U251 cells, at 72 h after transfection), whereas the transfection of the pathological hPHGDH variants produced a subtle and stable elevation of PSP, with the highest levels detected in U251

cells expressing V425M hPHGDH (as in the case of endogenous PSAT, a ~2-fold increase with respect to untransfected control cells was observed). Notably, at 72 h after transfection, the cellular levels of PSP were only restored in U251 cells expressing the V490M variant.

Immunofluorescence analysis of over-expressed hPHGDH variants distribution indicated that all were expressed in cytosol (Figure S9). However, the accumulation of V425M hPHGDH in large macromolecular aggregates was evident at all times after transfection: the observed aggregates/plaques colocalized with dense spots labeled by the DRAQ5 dye, which is specific for double strand DNA. These entities were observed only in transfected cells and were prevalent in those expressing V425M hPHGDH. Moreover, in a large fraction of U251 cells expressing this variant, the nucleus often appeared lobated and altered to different extent (Figure S9): this could represent a stress response induced by aggregates accumulation.

Most notably, double staining analysis performed by using anti-PSAT or anti-PSP antibodies showed that both these components of the PP were also entrapped within the V425M hPHGDH aggregates, since the corresponding fluorescent signals overlapped with the ectopically expressed hPHGDH variant and DRAQ5 ones (Figure 6). The same analysis showed that the over-expressed V261M and V490M variants partially colocalized with the endogenous PSAT and PSP proteins in the cytosol. The overlapping distribution was particularly evident in the transfected cells, where the cellular levels of the latter two proteins were higher. Therefore, hPHGDH overexpression induces a transient accumulation of PSAT and PSP at <48 h from transient transfection: the pathological variants (especially the V425M) favor aggregation and mistargeting of the three enzymes of the PP.

The actual correlation and the degree of colocalization of signals corresponding to the FLAG tagged hPHGDH variants (labeled in red) and total hPHGDH or endogenous PSAT and PSP (labeled in green) was evaluated by the Fiji software using the JACoP plugin. As expected, when the signal corresponding to the ectopically expressed hPHGDH variants and total hPHGDH were analyzed, the calculated M1 and M2 values (in the 0.60–0.85 range) indicated that they largely overlap. Accordingly, a high correlation of the signals was apparent based on r and correlation coefficient: mean values in the 0.40–0.80 and 0.60–0.85 range, respectively. The overlapping in signal pairs sensibly decreased when those corresponding to the overexpressed hPHGDH variants and the endogenous PSAT (M1 and M2 values in the 0.20–0.60 range) or PSP (M1 and M2 values in the 0.30–0.60 range) were evaluated. In line with these findings, the r and correlation coefficient mean values obtained for
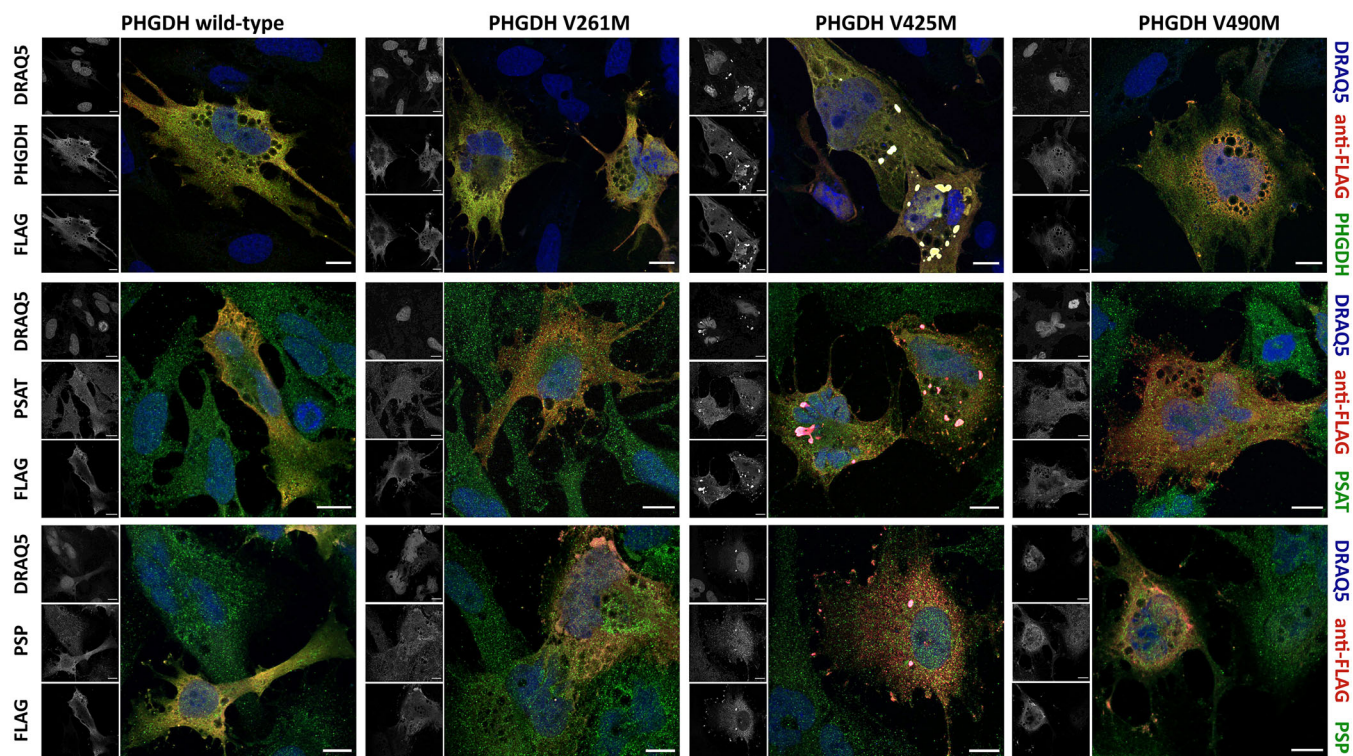
FIGURE 6 Confocal analysis of U251 cells showing the cellular distribution of the ectopically expressed hPHGDH variants (stained with the anti-FLAG antibody in red), relatively to the endogenous PP's proteins (stained by the anti-PHGDH, anti-PSAT, and anti-PSP antibody, respectively, in green). In the case of anti-PHGDH antibody, the obtained stain corresponds to the total (ectopically and endogenously expressed) hPHGDH protein and a colocalization of signals is evident between endogenous hPHGDH and FLAG-tagged recombinant variants. A partial colocalization is also observed with endogenous PSAT and PSP, for all the overexpressed hPHGDH variants. Worthy of note, the signals of the endogenous PP's proteins clearly colocalize with hPHGDH V425M one in the large macromolecular aggregates produced as a consequence of the overexpression of this (largely insoluble) protein variant. Nuclei were stained with the DRAQ5 fluorescent dye (blue). Scale bar = 10 μm.

signals corresponding to the different hPHGDH variants and the endogenous PSAT and PSP were in the 0.30–0.45 and 0.35–0.55 range, respectively. This analysis shows that the overexpressed hPHGDH variants partially co-distribute with the endogenous PSAT and PSP proteins and that the correlation of the signals for different PP's enzymes couples is similar, albeit a clear colocalization in dense macromolecular aggregates is apparent for V425M hPHGDH.

The cellular L-Ser level at 24 h from transfection was lower for all cell lines overexpressing the hPHGDH pathological variants (in particular the V425M and V490M ones) compared with those ectopically expressing the wild-type dehydrogenase. Changes in L-Ser content are evident both when expressing the amino acid concentration relatively to the total protein or the total hPHGDH amount (Figure 7A). Since no significant difference in D-Ser levels were observed, an increased D-/total serine ratio was calculated for the cells ectopically expressing the pathological variants (Figure 7B,C). Notably, the change in Gly cellular content strictly resembled the L-

Ser one, that was lower in cells overexpressing pathological hPHGDH variants (Figure 7D). These observations strongly suggest that L-Ser biosynthesis is hampered by over-expressing the pathological V261M, V425M, and V490M hPHGDH variants.

Taken together, these findings are intriguing in view of the recently identified "serinosome,"[15] a functional cytosolic enzyme assembly deputed to L-Ser biosynthesis and involving the PP proteins. It is tempting to speculate that pathological mutations, such as the V425M substitution in hPHGDH strongly affecting the protein solubility, might exert their effect altering the clustering process and hampering the appropriate complex formation and functionality.

4 | DISCUSSION

In this work, the three hPHGDH variants corresponding to known pathological SNPs in which a valine (in position 261, 425, or 490) has been substituted by a

(A) L-Ser

(B) D-Ser

(C) D/(D+L)-Ser%

(D) Gly
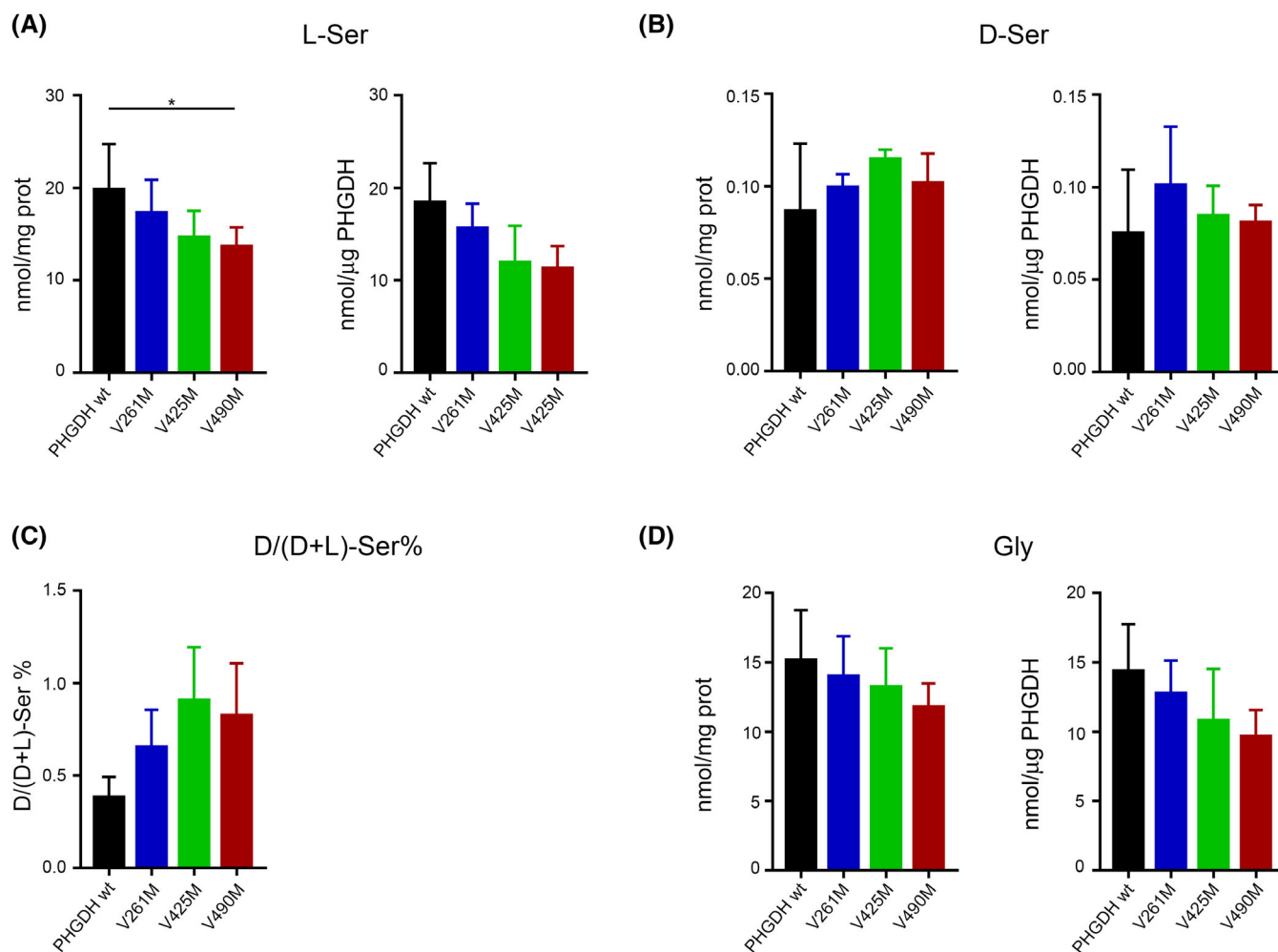
FIGURE 7 HPLC analysis of amino acids content of U251 cells overexpressing pathological hPHGDH variants at 24 h after transfection. The amount of amino acids (nmol) was normalized on the total protein or hPHGDH content. (A) L-Ser; (B) D-Ser; (C) D-/total Ser ratio; (D) Gly. Graphs report mean $\pm$ SEM ($n = 3$), analyzed by randomized blocks ANOVA and Dunnett's post hoc test. * $p < 0.05$.

methionine (Table 1) have been produced in a recombinant form and ectopically expressed in U251 cells; this with the aim to clarify the effect of such substitutions on the structure–function relationships of the enzyme, its cellular distribution and the PP functionality, that is, on L-Ser cellular levels.

All the three substitutions deeply alter hPHGDH secondary, tertiary and quaternary structure and significantly reduce protein solubility. This is made apparent by: (a) the accumulation of V425M and V490M variants as inclusion bodies when expressed in a recombinant form in *E. coli* cells; (b) the alteration of the spectroscopic signals (CD and fluorescence) related to the secondary and tertiary protein structure (Figure 3) and the higher accessibility of hydrophobic regions compared with the wild-type counterpart (as reported by titration with the probe ANS, see Table 3 and Figure S4); (c) the

absence of a clear unfolding transition in temperature ramp experiments (Figure S4). These alterations are also related to the larger oligomeric state and partial aggregation observed in solution for the variants compared with the classical tetrameric one of wild-type hPHGDH (Figure 4).[1] The predicted interaction of different hPHGDH subunits at the putative tetramerization domain (ASB-ACT) has the best reliability and a topology comparable to *M. tuberculosis* counterpart only when both ASB and ACT domains are modeled at the same time (Figure S10), suggesting that the fold disruption of any of these domains may affect proper tetramerization. Moreover, it is interesting to report that the AlphaFold-multimer modeled hPHGDH tetramer resembles that of MtPHGDH, suggesting ASB and ACT domains have preserved a similar role in regulating the tetramerization. Since the oligomerization state affects the hPHGDH

activity, the observed conformational alterations in the three pathological variants may impact on the kinetics of the reaction catalyzed by hPHGDH in the physiological direction and alter the K_m value for NADH (Table 2). Concerning the cofactor binding, and differently from the wild-type hPHGDH, the titration of the apoprotein with NADH is a monophasic process for all the pathological variants, with K_d values corresponding to the one determined for the second phase (at lower affinity) observed for the wild-type enzyme (Table 3). Although the largest decrease in apparent k_{cat} is determined for the V425M substitution (located in the ASB regulatory domain), the strongest decrease in kinetic efficiency (30–100 fold) is apparent for the V490M one (in the ACT regulatory domain), mainly due to a significant increase in K_m for 3PG and NAD^+. We highlight that the procedure based on refolding from inclusion bodies could also partially affect the kinetic properties of the V425M and V490M variants since a 3-fold lower specific activity was also apparent for the wild-type dehydrogenase when isolated from the insoluble fraction. Notably, kinetic parameters for the reverse reaction (frequently used in the past to assay hPHGDH activity, lacking a suitable assay in the forward direction),[38,39] were marginally affected by the substitutions ($\leq$8-fold, Table 2). This is a main point when comparing our results with previous investigations (see below).

At the cellular level, the alterations in protein stability and solubility observed for the hPHGDH pathological variants might have a dramatic effect on the assembly process and the functionality of the serinosome.[15] To further investigate this hypothesis, the wild-type, V261M, V425M, and V490M hPHGDH variants were ectopically expressed in U251 cells. Notably, and differently from the wild-type enzyme, the pathological variants were partially mistargeted to the nucleus and induced the formation of large molecular aggregates that contained PSAT and PSP too (Figures 6 and S9): this was particularly evident for the V425M hPHGDH. As a general rule, overexpression of hPHGDH pathological variants induced a transient accumulation of PSAT and PSP: this could result from their assembly in the serinosome. Notwithstanding the increase in cellular levels of the PP enzymes, the expression of all three pathological variants led to a decrease in L-Ser and Gly cellular concentrations (Figure 7), demonstrating their relevant role in L-Ser levels decrease observed in patients. Indeed, the co-localization of the three enzymes of the PP even for the pathological variants suggests that the substitutions are located in hPHGDH regions that do not hinder the protein recognition with PSAT and PSP.

Previous studies reported that the expression of V425M and V490M variants in reticulocyte lysates did not alter the expression levels and protein turnover compared with the wild-type hPHGDH.[38] Using fibroblast lysates from affected patients, the reaction rate in the reverse direction was halved for these variants compared with the wild-type enzyme, with no change in apparent K_m for 3PHP. Later on, the main pathological effect of the V490M amino acid substitution has been linked to impairment of protein folding and/or assembly, with limited effect on activity and stability of the portion of protein that reached the final, mature conformation.[39] Compared with (partial) enzymatic inactivation, the misfolding/aggregation of hPHGDH pathological V425M and V490M variants should better explain the severity of the neurological and developmental impairments observed in affected patients.

The missense mutation yielding to the V261M substitution in the cofactor binding domain was also reported in a Turkish boy identified for severe low blood L-Ser and Gly concentrations.[40] The level of expression in fibroblasts did not differ between the V261M variant and the wild-type hPHGDH, as well as the maximal apparent activity of the reverse reaction, but a 4-fold increased K_m for 3PHP and a substrate inhibition at concentrations >400 μM was apparent. We now clearly establish that the evaluation of the hPHGDH reverse reaction did not resemble the pathological effect of such mutation(s) in the physiological direction and thus understated the decrease in the kinetic efficiency.

Briefly, it is not possible to attribute the pathological impact of the investigated hPHGDH variants (reported in a homozygous state)[18,38,40] solely to altered cellular expression levels: we propose that the pathological variants promote the generation of a poorly functional serinosome (making L-Ser biosynthesis less efficient) entrapping the other components of the PP and preventing their degradation.

Concerning the therapeutic approaches, previous studies demonstrated that the pharmacological supplementation of L-Ser in PHGDH deficiencies could ameliorate some of the related symptoms.[19] Anyway, and because of the low permeability of serine at brain–blood barrier, it does not represent a well-suited approach alone, since in the brain astrocytes L-Ser is the precursor of the NMDA receptor coagonist D-Ser and it is related to the levels of Gly, the alternative co-agonist. The characterization of pathological V261M, V425M, and V490M hPHGDH variants suggests the use of alternative approaches, such as acting on: (a) the protein folding, by using pharmacological chaperones to push protein fold-

ing, correct oligomerization, and acquisition of the catalytically competent conformation; (b) the enzymatic activity, by identifying allosteric modulators able to stimulate the activity, also by acting on the serinosome assembly process; (c) the metabolism, by altering glucose availability to push the diversion of 3PG from glycolysis to the PP; (d) D-Ser availability (which is produced by serine racemase using the corresponding L-enantiomer), for example, by inhibiting the catabolic enzyme D-amino acid oxidase.[41]

AUTHOR CONTRIBUTIONS

Loredano Pollegioni and Giulia Murtas conceived the work, designed the experiments and drafted the article. Giulia Murtas, Valentina Rabattoni and Laura Caldinelli performed the preparation and the biochemical characterization of protein variants. Zoraide Motta and Elena Zerbini performed the HPLC analyses. Silvia Sacchi and Elena Zerbini performed cellular studies. Marco Orlando contributed to the structural prediction analysis. Barbara Campanini and Francesco Marchesani prepared PSAT and PSP proteins. All authors contributed to the analysis and discussion of the results and critically revised the manuscript. All authors have read and agreed to the published version of the manuscript.

ACKNOWLEDGMENTS

CONFLICT OF INTEREST STATEMENT

The authors declare no conflict of interest.

DATA AVAILABILITY STATEMENT

Data available on request from the authors.

ORCID

Loredano Pollegioni https://orcid.org/0000-0003-1733-7243

REFERENCES

1. Murtas G, Marcone GL, Sacchi S, Pollegioni L. L-serine synthesis via the phosphorylated pathway in humans. Cell Mol Life Sci. 2020;77(24):5131–48. https://doi.org/10.1007/s00018-020-03574-z

2. Grant GA. Contrasting catalytic and allosteric mechanisms for phosphoglycerate dehydrogenases. Arch Biochem Biophys. 2012;519((2)):175–85. https://doi.org/10.1016/j.abb.2011.10.005

3. Murtas G, Marcone GL, Peracchi A, Zangelmi E, Pollegioni L. Biochemical and biophysical characterization of recombinant human 3-phosphoglycerate dehydrogenase. Int J Mol Sci. 2021;22(8):4231. https://doi.org/10.3390/ijms22084231

4. Yang M, Vousden KH. Serine and one-carbon metabolism in cancer. Nat Rev Cancer. 2016;16(10):650–62. https://doi.org/10.1038/nrc.2016.81

5. Yang JH, Wada A, Yoshida K, Miyoshi Y, Sayano T, Esaki K, et al. Brain-specific *Phgdh* deletion reveals a pivotal role for L-serine biosynthesis in controlling the level of D-serine, an N-methyl-D-aspartate receptor co-agonist, in adult brain. J Biol Chem. 2010;285(53):41380–90. https://doi.org/10.1074/jbc.M110.187443

6. Pollegioni L, Sacchi S. Metabolism of the neuromodulator D-serine. Cell Mol Life Sci. 2010;67(14):2387–404. https://doi.org/10.1007/s00018-010-0307-9

7. Amelio I, Cutruzzolá F, Antonov A, Agostini M, Melino G. Serine and glycine metabolism in cancer. Trends Biochem Sci. 2014;39(4):191–8. https://doi.org/10.1016/j.tibs.2014.02.004

8. Mattaini KR, Sullivan MR, Vander Heiden MG. The importance of serine metabolism in cancer. J Cell Biol. 2016;214(3):249–57. https://doi.org/10.1083/jcb.201604085

9. Murtas G, Pollegioni L. D-amino acids and cancer: friends or foes? Int J Mol Sci. 2023;24(4):3274. https://doi.org/10.3390/ijms24043274

10. Rathore R, Schutt CR, Van Tine BA. PHGDH as a mechanism for resistance in metabolically-driven cancers. Cancer Drug Resist. 2020;3(4):762–74. https://doi.org/10.20517/cdr.2020.46

11. Grant GA. D-3-phosphoglycerate dehydrogenase. Front Mol Biosci. 2018;5:110. https://doi.org/10.3389/fmolb.2018.00110

12. Xu XL, Chen S, Salinas ND, Tolia NH, Grant GA. Comparison of type 1 D-3-phosphoglycerate dehydrogenases reveals unique regulation in pathogenic mycobacteria. Arch Biochem Biophys. 2015;570:32–9. https://doi.org/10.1016/j.abb.2015.02.008

13. Dey S, Grant GA, Sacchettini JC. Crystal structure of *Mycobacterium tuberculosis* D-3-phosphoglycerate dehydrogenase: extreme asymmetry in a tetramer of identical subunits. J Biol Chem. 2005;280(15):14892–9. https://doi.org/10.1074/jbc.M414489200

14. Jumper J, Evans R, Pritzel A, Green T, Figurnov M, Ronneberger O, et al. Highly accurate protein structure prediction with AlphaFold. Nature. 2021;596(7873):583–9. https://doi.org/10.1038/s41586-021-03819-2

15. Rabattoni V, Marchesani F, Murtas G, Sacchi S, Mozzarelli A, Bruno S, et al. The human phosphorylated pathway: a multienzyme metabolic assembly for L-serine biosynthesis. FEBS J. 2023;290:3877–95. https://doi.org/10.1111/febs.16787

16. Jaeken J, Detheux M, Van Maldergem L, Foulon M, Carchon H, van Schaftingen E. 3-Phosphoglycerate dehydrogenase deficiency: an inborn error of serine biosynthesis. Arch Dis Child. 1996;74(6):542–5. https://doi.org/10.1136/adc.74.6.542

17. de Koning TJ, Duran M, Dorland L, Gooskens R, van Schaftingen E, Jaeken J, et al. Beneficial effects of L-serine and glycine in the management of seizures in 3-phosphoglycerate dehydrogenase deficiency. Ann Neurol. 1998;44(2):261–5. https://doi.org/10.1002/ana.410440219

18. Pineda M, Vilaseca MA, Artuch R, Santos S, García González MM, Aracil A, et al. 3-Phosphoglycerate dehydrogenase deficiency in a patient with west syndrome. Dev Med Child Neurol. 2000;42(9):629–33. https://doi.org/10.1017/s0012162200001171

19. Tabatabaie L, Klomp LW, Rubio-Gozalbo ME, Spaapen LJ, Haagen AA, Dorland L, et al. Expanding the clinical spectrum of 3-phosphoglycerate dehydrogenase deficiency. J Inherit Metab Dis. 2011;34(1):181–4. https://doi.org/10.1007/s10545-010-9249-5

20. Ni C, Cheng RH, Zhang J, Liang JY, Wei RQ, Li M, et al. Novel and recurrent PHGDH and PSAT1 mutations in Chinese patients with Neu-Laxova syndrome. Eur J Dermatol. 2019;29(6):641–6. https://doi.org/10.1684/ejd.2019.3673

21. Eade K, Gantner ML, Hostyk JA, Nagasaki T, Giles S, Fallon R, et al. Serine biosynthesis defect due to haploinsufficiency of PHGDH causes retinal disease. Nat Metab. 2021;3(3):366–77. https://doi.org/10.1038/s42255-021-00361-3

22. Liu H, Naismith JH. An efficient one-step site-directed deletion, insertion, single and multiple-site plasmid mutagenesis protocol. BMC Biotechnol. 2008;8:91. https://doi.org/10.1186/1472-6750-8-91

23. Caldinelli L, Molla G, Bracci L, Lelli B, Pileri S, Cappelletti P, et al. Effect of ligand binding on human D-amino acid oxidase: implications for the development of new drugs for schizophrenia treatment. Protein Sci. 2010;19(8):1500–12. https://doi.org/10.1002/pro.429

24. Molla G, Porrini D, Job V, Motteran L, Vegezzi C, Campaner S, et al. Role of arginine 285 in the active site of Rhodotorula gracilis D-amino acid oxidase. A site-directed mutagenesis study. J Biol Chem. 2000;275(32):24715–21. https://doi.org/10.1074/jbc.M908193199

25. Caldinelli L, Iametti S, Barbiroli A, Bonomi F, Piubelli L, Ferranti P, et al. Unfolding intermediate in the peroxisomal flavoprotein D-amino acid oxidase. J Biol Chem. 2004;279(27):28426–34. https://doi.org/10.1074/jbc.M403489200

26. Caldinelli L, Molla G, Sacchi S, Pilone MS, Pollegioni L. Relevance of weak flavin binding in human D-amino acid oxidase. Protein Sci. 2009;18(4):801–10. https://doi.org/10.1002/pro.86

27. Sacchi S, Lorenzi S, Molla G, Pilone MS, Rossetti C, Pollegioni L. Engineering the substrate specificity of D-amino-acid oxidase. J Biol Chem. 2002;277(30):27510–6. https://doi.org/10.1074/jbc.M203946200

28. Fiser A, Do RK, Sali A. Modeling of loops in protein structures. Protein Sci. 2000;9(9):1753–73. https://doi.org/10.1110/ps.9.9.1753

29. Webb B, Sali A. Protein structure modeling with MODELLER. Methods Mol Biol. 2014;1137:1–15. https://doi.org/10.1007/978-1-4939-0366-5_1

30. Kaynak BT, Zhang S, Bahar I, Doruker P. ClustENMD: efficient sampling of biomolecular conformational space at atomic resolution. Bioinformatics. 2021;37(21):3956–8. https://doi.org/10.1093/bioinformatics/btab496

31. Bakan A, Meireles LM, Bahar I. ProDy: protein dynamics inferred from theory and experiments. Bioinformatics. 2011;27(11):1575–7. https://doi.org/10.1093/bioinformatics/btr168

32. Eastman P, Swails J, Chodera JD, McGibbon RT, Zhao Y, Beauchamp KA, et al. OpenMM 7: rapid development of high performance algorithms for molecular dynamics. PLoS Comput Biol. 2017;13(7):e1005659. https://doi.org/10.1371/journal.pcbi.1005659

33. Maier JA, Martinez C, Kasavajhala K, Wickstrom L, Hauser KE, Simmerling C. ff14SB: improving the accuracy of protein side chain and backbone parameters from ff99SB. J Chem Theory Comput. 2015;11(8):3696–713. https://doi.org/10.1021/acs.jctc.5b00255

34. Tiberti M, Terkelsen T, Degn K, Beltrame L, Cremers TC, da Piedade I, et al. MutateX: an automated pipeline for in silico saturation mutagenesis of protein structures and structural ensembles. Brief Bioinform. 2022;23((3)):bbac074. https://doi.org/10.1093/bib/bbac074

35. Delgado J, Radusky LG, Cianferoni D, Serrano L. FoldX 5.0: working with RNA, small molecules and a new graphical interface. Bioinformatics. 2019;35(20):4168–9. https://doi.org/10.1093/bioinformatics/btz184

36. Xu H, Qing X, Wang Q, Li C, Lai L. Dimerization of PHGDH via the catalytic unit is essential for its enzymatic function. J Biol Chem. 2021;296:100572. https://doi.org/10.1016/j.jbc.2021.100572

37. Volontè F, Marinelli F, Gastaldo L, Sacchi S, Pilone MS, Pollegioni L, et al. Optimization of glutaryl-7-aminocephalosporanic acid acylase expression in E. coli. Protein Expr Purif. 2008;61(2):131–7. https://doi.org/10.1016/j.pep.2008.05.010

38. Klomp LW, de Koning TJ, Malingré HE, van Beurden EA, Brink M, Opdam FL, et al. Molecular characterization of 3-phosphoglycerate dehydrogenase deficiency – a neurometabolic disorder associated with reduced L-serine biosynthesis. Am J Hum Genet. 2000;67(6):1389–99. https://doi.org/10.1086/316886

39. Pind S, Slominski E, Mauthe J, Pearlman K, Swoboda KJ, Wilkins JA, et al. V490M, a common mutation in 3-phosphoglycerate dehydrogenase deficiency, causes enzyme deficiency by decreasing the yield of mature enzyme. J Biol Chem. 2002;277(9):7136–43. https://doi.org/10.1074/jbc.M111419200

40. Tabatabaie L, de Koning TJ, Geboers AJ, van den Berg IE, Berger R, Klomp LW. Novel mutations in 3-phosphoglycerate dehydrogenase (PHGDH) are distributed throughout the protein and result in altered enzyme kinetics. Hum Mutat. 2009;30(5):749–56. https://doi.org/10.1002/humu.20934

41. Pollegioni L, Sacchi S, Murtas G. Human D-amino acid oxidase: structure, function, and regulation. Front Mol Biosci. 2018;5:107. https://doi.org/10.3389/fmolb.2018.00107

42. Shaheen R, Rahbeeni Z, Alhashem A, Faqeih E, Zhao Q, Xiong Y, et al. Neu-Laxova syndrome, an inborn error of serine metabolism, is caused by mutations in PHGDH. Am J Hum Genet. 2014;94(6):898–904. https://doi.org/10.1016/j.ajhg.2014.04.015

43. Richards S, Aziz N, Bale S, Bick D, Das S, Gastier-Foster J, et al. Standards and guidelines for the interpretation of sequence variants: a joint consensus recommendation of the American College of Medical Genetics and Genomics and the Association for Molecular Pathology. Genet Med. 2015;17(5):405–24. https://doi.org/10.1038/gim.2015.30

44. Acuna-Hidalgo R, Schanze D, Kariminejad A, Nordgren A, Kariminejad MH, Conner P, et al. Neu-Laxova syndrome is a heterogeneous metabolic disorder caused by defects in enzymes of the L-serine biosynthesis pathway. Am J Hum Genet. 2014;95(3):285–93. https://doi.org/10.1016/j.ajhg.2014.07.012

45. El-Hattab AW, Shaheen R, Hertecant J, Galadari HI, Albaqawi BS, Nabil A, et al. On the phenotypic spectrum of serine biosynthesis defects. J Inherit Metab Dis. 2016;39(3): 373–81. https://doi.org/10.1007/s10545-016-9921-5

46. Adzhubei IA, Schmidt S, Peshkin L, Ramensky VE, Gerasimova A, Bork P, et al. A method and server for predicting damaging missense mutations. Nat Methods. 2010;7(4): 248–9. https://doi.org/10.1038/nmeth0410-248

47. Zhang H, Xu MS, Fan X, Chung WK, Shen Y. Predicting functional effect of missense variants using graph attention neural networks. Nat Mach Intell. 2022;4:1017–28. https://doi.org/10.1038/s42256-022-00561-w

48. Hekkelman ML, de Vries I, Joosten RP, Perrakis A. AlphaFill: enriching AlphaFold models with ligands and cofactors. Nat Methods. 2023;20(2):205–13. https://doi.org/10.1038/s41592-022-01685-y

SUPPORTING INFORMATION

Additional supporting information can be found online in the Supporting Information section at the end of this article.